PCCP

ARTICLE TYPE

Cite this: DOI: 00.0000/xxxxxxxxxx

Simple corrections for the static dielectric constant of liquid mixtures from model force fields†

Javier Cardona,*[ab] Miguel Jorge,[a] and Leo Lue[a]

Received Date
Accepted Date

DOI: 00.0000/xxxxxxxxxx

Pair-wise additive force fields provide fairly accurate predictions, through classical molecular simulations, for a wide range of structural, thermodynamic, and dynamical properties of many materials. However, one key property that has not been well captured is the static dielectric constant, which characterizes the response of a system to an applied electric field and is important in determining the screening of electrostatic interactions through a system. A simple correction has been found to provide a relatively robust method to improve the estimate of the static dielectric constant from molecular simulations for a broad range of compounds. This approach accounts for the electronic contribution to molecular polarizability and assumes that the charges that couple a molecule to an applied electric field are proportional to the effective force field charges. In this work, we examine how this correction performs for systems at different temperatures and for binary mixtures. Using a value for the electronic polarizability, based on the experimental index of refraction, and a charge scaling factor, determined at a single temperature, we find that the static dielectric constant can be predicted remarkably well, in comparison to the experimentally measured values. This provides good evidence that the effective charges that appear in pair-wise additive force fields developed to reproduce the potential energy surface of a system are not the same as those that determine the static dielectric constant; however, they can be captured in a relatively simple manner, which is dependent on the particular force field.

1 Introduction

Molecular simulations have developed tremendously over the past decades. They have become an extremely useful tool for not only making quantitative predictions for a wide range of material properties, but also providing insight into the microscopic processes that lead to these properties. The accuracy of the results of the simulations depends crucially on the force fields used to describe the geometry of the molecules that compose the system and the interactions between them. The "exact" force fields that act between molecules are complicated, multi-body functions, which are not precisely known. In order to minimize the parameters required to characterize a model force field and the computational requirements for its evaluation, the energy surface of a molecular system is usually approximated by describing molecules as collections of point interaction sites, representing atoms or groups of atoms, which interact through pair-wise additive potentials.

While this approximation is quite dramatic, it does provide a relatively robust framework for constructing model force fields that give good predictions for thermodynamic and mechanical properties of fluids and are fairly transferable across different chemical systems. Examples of these kinds of force fields include OPLS[1,2], TraPPE-UA[3–9] and TraPPE-EH[10,11], CHARMM[12], AMBER[13,14], GROMOS[15], etc. These force fields are typically parameterized to accurately reproduce the structural, thermodynamic, and transport properties of a wide variety of liquid systems.

While these pair potential models have been quite successful in describing a wide range of thermodynamic, structural, and dynamic properties, one key property that has not been well captured is the static dielectric constant[16–20]. The static dielectric constant ε describes the manner in which solvents "screen" electrostatic interactions. It is directly related to fluctuations in the total dipole moment $\mathbf{M}$ of the system[21,22]

$$\varepsilon_{\mathrm{PES}} = 1 + \frac{4\pi}{3k_B T\langle V\rangle}(\langle|\mathbf{M}|^2\rangle - |\langle\mathbf{M}\rangle|^2) \quad (1)$$

where V is the volume of the system, T is the absolute temperature, and k_B is the Boltzmann constant. These fluctuations are due to the motion of charges in the system and govern the man-

[a] Department of Chemical and Process Engineering, University of Strathclyde, James Weir Building, 75 Montrose Street, Glasgow G1 1XJ, United Kingdom; E-mail: j.cardona-amengual@strath.ac.uk

[b] Department of Electronic and Electrical Engineering, University of Strathclyde, Royal College Building, 204 George Street, Glasgow G1 1XW, United Kingdom.

† Electronic Supplementary Information (ESI) available: Influence of temperature on the static dielectric constant of single component systems; Dipole moment distributions for single component systems; Influence of temperature on the infinite frequency dielectric constant; Influence of temperature on the density of single component systems and binary mixtures. See DOI: 10.1039/cXCP00000x/

ner in which it couples to weak, externally applied electric fields. The charges are due to the nuclei and electrons that compose the molecules in the system. The subscript PES in the above equation means that the charges of the model used to compute the dielectric constant were optimized to reproduce the potential energy surface (PES) of the pure liquid.

Indeed, a crucial element of the parameterization of pairwise additive force fields includes the assignment of fixed point charges to the interaction sites within the molecules of the system. The effective charges used in a particular force field, which are designed to describe the PES of the liquid, may not be the same as the charges that would most accurately reflect the molecule's polarization state in that liquid (partly due to fixed charges and partially due to polarization by neighboring molecules)[23]. In fact, as argued by Leontyev and Stuchebrukhov[24–26] the force field charges (and hence the dipole moment of the molecular model) can be interpreted as effective scaled charges, that are adjusted down from the charges that would represent the real liquid dipole moment. This is one of the reasons why most fixed-charge force fields have dipole moments that are approximately half-way between the gas and the liquid dipole moments[27–30] A direct consequence of this choice is that fixed-charge force fields are then unable to accurately predict properties that depend directly on the dipole moment surface (DMS), such as the dielectric constant[23,30,31].

Recently, a simple method was proposed to correct the predictions of fixed-charge force fields for polarization effects by scaling the apparent charges by a constant term[31]. First, the magnitude of the charges that couple the molecule to an applied external field are assumed to be proportional to the magnitude of the charges that effectively represent the electrostatic interactions between molecules:

$$k = \frac{q_{\mathrm{DMS}}}{q_{\mathrm{PES}}} \tag{2}$$

where k is a proportionality constant, q_{DMS} is the scaled charge to represent the dipole moments of the molecules in the system, and q_{PES} is the assigned charge to represent the potential energy surface. In essence, this compensates for the scaling of the charges that is implicit in models designed to fit the PES and allows for better estimation of properties that rely on the DMS. The scaling is applied as a post-processing step to recalculate the DMS-dependent properties, while all the PES-dependent properties are identical to those of the original force field.

In addition to this effect, fixed-charge force fields also omit the contribution of purely electronic fluctuations to the dielectric constant. Assuming that these fluctuations are much faster than the nuclear component of the dielectric response (which is equivalent to the Born-Oppenheimer approximation), the influence of these electronic fluctuations can be thought of as contributing an additional uniform polarization density to the system, which would simply result in replacing the 1 in Eq. (1) with ε_∞. A common way to estimate ε_∞ is to relate it to the refractive index of the medium, measured at the sodium D-line frequency n_D, via $\varepsilon_\infty = n_D^2$; at these high frequencies, only the electronic contribution is measurable, and therefore the high-frequency dielectric constant is, at least in principle, an experimentally accessible property.

If ε_{PES}, given by Eq. (1), is obtained from a classical simulation using the fixed-charge effective dipoles, and ε_{DMS} corresponds to the actual dielectric constant of the liquid using dipoles scaled by Eq. (2) and shifting the background polarizability, we can obtain a simple expression that allows us to estimate the experimental dielectric constant from ε_{PES}:

$$\varepsilon_{\mathrm{DMS}} = \varepsilon_\infty + k^2(\varepsilon_{\mathrm{PES}} - 1) \tag{3}$$

A value of $k = 1.26$ for the scaling factor was found to give reasonable predictions of the static dielectric constant for a wide range of pure liquids described by different molecular models[31].

This idea is supported by the further observations that the experimental time autocorrelation of the system dipole moment can be fairly well captured by molecular dynamics simulations[32–34], even if the static dielectric constant is not well reproduced. In previous work, we stated the importance of using appropriate values of the static dielectric constant ε_0 and the infinite frequency permittivity ε_∞ for the determination of dielectric spectra, in particular to obtain a good estimate of the intensity of the main absorption peak observed in the dielectric loss. In this work, we examine the robustness of this idea by understanding how the method performs for systems at different temperatures and for mixtures.

The remainder of this paper is organized as follows. The next section presents the details of the force fields used to describe the intermolecular interactions for the systems we examine, as well as the molecular dynamics simulations, and the analysis methods. Results for single component systems at variable temperature are presented in the following section. We then move on to mixtures, in particular, ethanol-water solutions and ethanol-benzene solutions. Finally, the main findings of the paper are summarized, along with a discussion of directions for future work.

2 Simulation details

In this work, molecular dynamics (MD) simulations are performed to test the correction scheme on the prediction of static dielectric constants of the binary mixtures ethanol-water and ethanol-benzene using non-polarisable models. The robustness of the scheme to temperature variations is also investigated. Two models are examined for water: TIP4P[35] and SPC-Fw[36]. The TIP4P model is a rigid model consisting of four sites: one located at the oxygen atom, one located at each of the hydrogen atoms and one additional site situated along the bisector of the H-O-H bond angle, improving the electrostatic distribution around the molecule. This widely used model is selected since it provides reasonable predictions for thermodynamic properties but happens to have a poor performance at estimating the static dielectric constant[37]. In contrast, the SPC-Fw water model provides a more accurate prediction of this property. In this work, a modified version of the SPC-Fw model, which has been used by the authors in previous studies[32,33], is implemented. Through this approach, bond stretching is suppressed but the bond angle is still allowed to fluctuate, respecting the conclusions reached during the development of the original model, by which angle bending has consid-

erably larger influence on the static dielectric constant than bond stretching[36].

The Transferable Potentials for Phase Equilibria (TraPPE) force field is used to describe ethanol and benzene. The TraPPE-UA model[6,7] used for ethanol implements a semi-flexible approach, with suppression of bond stretching but allowing bond angle bending. In contrast, benzene is represented by a fully rigid model through the TraPPE-EH force field[11].

All molecular dynamics simulations were performed using GROMACS version 2019.3[38] in the NpT ensemble using a velocity scaling thermostat[39] with a time constant of 0.1 ps and the Parrinello-Rahman barostat[40,41] with a time constant of 1.0 ps and a compressibility of 4.5×10^{-5} bar^{-1}. All simulations were performed at a pressure of 1 bar. The long-range contributions to the electrostatic interactions were calculated using smooth particle mesh Ewald[42], and bond length constraints were maintained using the LINCS algorithm[43]. The equations of motion were integrated using the leap-frog algorithm with a time step of 1 fs.

All of the systems examined in this work consist of $N = 1000$ molecules. To obtain statistically independent starting configurations, initial simulations were performed at a temperature of 340 K for each composition, and four configurations were selected at 1 ns intervals. From each of these configurations, an equilibration run of 2 ns was performed at the target temperature, followed by a 10 ns production run where properties are collected. The values reported for the properties are averages over the four independent runs, with uncertainties estimated from the corresponding standard deviations. Input files for all simulations performed in this work are openly available from the University of Strathclyde KnowledgeBase at https://doi.org/10.15129/df052d7c-5106-4793-8a39-6765c068e8af.

3 Results and discussion

3.1 Single component systems

The variation of the static dielectric constant ε_0 with temperature for pure benzene, ethanol, and water is shown in Fig. 1(a). The open symbols are experimental data for benzene[49,54–57], ethanol[44,48–53], and water[44–49]. The filled symbols are from the MD simulations. The static dielectric constant gives the polarization of a system in response to an externally applied electric field. Systems which can more strongly couple to this field to align their induced and molecular dipoles will have a larger value of ε_0.

The dipole moments of each of the molecules, along with some other molecular properties, are shown in Table 1. The quantity χ is the electronic polarizability, n_D is the index of refraction at the sodium-D line, k is the charge scaling factor, μ_{gas} is the dipole moment in the gas phase, μ_{PES} is the dipole moment of the force field model. The corresponding dipole moment distributions calculated from our MD simulations are presented in Fig. S2 of the ESI†. Molecules with larger dipole moments are expected to have a larger static dielectric constant[58]. Water and ethanol, which both possess permanent dipoles, have a significantly larger static dielectric constant than benzene, which does not posses a permanent dipole. For these polar systems, the main response to an applied electric field is to rotate the constituent molecules in order to orient their dipoles with the field. In cases where molecular orientations are uncorrelated (or only weakly correlated), larger dipole moments result directly in larger values of the static dielectric constant. Correlations between molecules which arise from their interactions can enhance the collective alignment of their dipoles and have the potential to further increase the static dielectric constant of the system. The larger values of ε_0 for water are a consequence of the hydrogen bond networks that form between molecules, which lead to clusters where the dipole moments of the individual molecules are fairly correlated and result in relatively larger fluctuations in overall net dipole moment of the system[59]. These coherent networks are not present in ethanol[60–62].

Benzene has the lowest static dielectric constant, which is a consequence of its lack of a permanent dipole. Its main response to an applied electric field is due to the electronic polarizability of the molecules, where the electron distribution of the molecules deforms, resulting in an induced dipole moment. The magnitude of this induced dipole, however, is typically much smaller than that of the permanent dipoles of polar molecules.

The force fields used were mainly parameterized to reproduce thermodynamic properties[6,10,11,35]. As a consequence, they are not necessarily expected to yield accurate dielectric properties. In general, the simulation data lie beneath the experimentally measured values. The modified SPC-Fw model is an exception, which

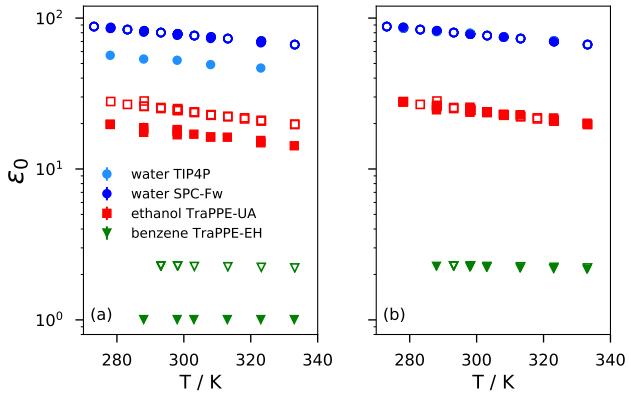

Fig. 1 Influence of temperature on the static dielectric constant ε_0 of water, ethanol and benzene at 1 bar. Filled symbols represent results obtained in our simulations (a) before and (b) after applying the suggested correction scheme. The data points corresponding to water TIP4P and SPC-Fw overlap in (b) and only the latter are visible on the figure. Open symbols correspond to experimental measurements from different sources for water[44–49], ethanol[44,48–53], and benzene[49,54–57]. Note that the y-axis is shown on a logarithmic scale for ease of visualization. A version in linear scale can be found in Fig. S1 of the ESI†.

Table 1 Summary of molecular properties

	χ / Å^3	n_D‡	k	μ_{gas}‖ / D	μ_{PES} / D
water (TIP4P)	1.47[63]	1.3325	1.229	1.85	2.18
water (SPC-Fw)	1.47[63]	1.3325	1.005	1.85	2.34
ethanol	5.13[64,65]	1.3594	1.176	1.69	2.26
benzene	10.44[66]	1.4979	—	0.00	0.00

‡Measured at 25°C. Taken from Ref. 64.
‖Taken from Ref. 67.

appears to reproduce the experimental dielectric constant of water fairly well, as reported previously[32,33]. The agreement in the predictions of the TIP4P force field for water and the TraPPE-UA force field for ethanol are somewhat weaker, although the trends with temperature are maintained to a reasonable level.

The TIP4P model for water is fully rigid and has a constant dipole moment value of 2.18 D, while the dipole moment of the SPC-Fw model has a value of 2.34 D and only decreases slightly with temperature (see Fig. S2(b) of the ESI†). Although the dipole moment of the TIP4P model is only about 10% lower than that of the SPC-Fw model, its dielectric constant is about 30% lower. This shows that the magnitude of the molecular dipole moment is not the only factor that controls the dielectric constant.

The model for ethanol is flexible, able to bend its bond angles and rotate its dihedral angle that involves the hydroxyl group; however, the mean dipole moment of the molecule remains essentially constant with temperature at 2.26 D, as shown in Fig. S2(c) of the ESI†. Although its dipole moment is comparable to that of the water models, it yields a significantly lower dielectric constant. This is mainly because of the stronger correlation between dipoles in water due to the formation of three-dimensional hydrogen bond networks, resulting in larger fluctuations in the net dipole moment of the system.

Benzene has a dielectric constant that is only slightly above the vacuum value. The TraPPE-EH force field model for benzene is perfectly rigid, with a dipole moment that is exactly zero, and consequently, the dielectric constant from the simulation should be exactly equal to 1. In our MD simulations of the TraPPE-EH force field, the model was implemented with very stiff bending potentials, rather than rigid constraints, which led to a small fluctuation in the dipole moment with a root mean square fluctuation increasing from 0.074 to 0.080 D across the range of temperatures examined (see Fig. S2(d) of the ESI†), although the mean dipole moment is zero due to symmetry. This resulted in a slightly positive deviation from the vacuum value of the static dielectric constant, although its maximum value was less than 1.005.

In Fig. 1(b), the simulation data are shifted according to Eq. (3), which includes the corrections from electronic polarizability, where the vacuum permittivity is replaced by the infinite frequency dielectric constant ε_∞, and from rescaling the fixed charges by k.

The Clausius-Mossotti relation[68,69] provides an estimate for the electronic polarizability χ

$$\chi = \frac{3}{4\pi\rho}\frac{\varepsilon_\infty - 1}{\varepsilon_\infty + 2}, \tag{4}$$

where ρ is the number density of the molecules. This relation can be rearranged as

$$\varepsilon_\infty = 1 + \frac{4\pi\rho\chi}{1 - 4\pi\rho\chi/3} \tag{5}$$

which allows the prediction of the temperature and pressure dependence of ε_∞ given knowledge of χ. While the density depends on the temperature and pressure of the system, the electronic polarizability is expected to be essentially constant. Alternatively, we can use the refractive index at the sodium D-line to estimate the infinite frequency static dielectric constant (i.e. $\varepsilon_\infty \approx n_D^2$).

For all three liquids, the experimental value of ε_0 decreases with increasing temperature. In the case of polar molecules, such as water and ethanol, at high temperatures, the thermal motion of the molecules tends to disrupt the alignment of their dipole moments with an applied electric field, which thereby lowers the static dielectric constant. For benzene, the slight flexibility of the molecule leads to small, transient net dipole moments, which, taken on its own, would cause the dielectric constant to increase with temperature. This is opposite to what is experimentally observed; the dielectric constant is 2.28 at 20°C and drops to 2.19 at 70°C. Thus, the temperature dependence on the static dielectric constant of benzene is due to the influence of temperature on ε_∞ (see Fig. S3 of the ESI†). The electronic contribution to the static dielectric constant arises from the deformation of the electron distribution of individual molecules in response to an applied electric field, and, therefore, it is expected to be proportional to the number density of molecules in the system. The main cause for the decrease of ε_0 with increasing temperature is the decrease in density with temperature, as shown in Fig. S4(d) of the ESI†. As benzene has no permanent dipole moment, charge scaling has no impact on the prediction of dielectric constant, and the only correction is due to the electronic polarizability of the molecule. The addition of this contribution significantly improves the agreement of the simulation data with the experimental values.

The TraPPE-UA force field for ethanol underpredicts the static dielectric constant by about 25% across the range of temperatures that are considered. The correction to ε_0 is computed by adding the contribution due to electronic polarizability and adjusting a single, temperature independent value for the force field charge scaling factor k to obtain the best fit to the experimental data. With $k = 1.176$, the corrected simulation data agree quite well with the experimentally measured values across the entire temperature range from 0°C to 60°C. This value is close to the value $k = 1.26$[31], which was fit especially to the GAFF/AM-1-BCC model for methanol and found to give a reasonable description of the experimental static dielectric constant for a wide range of alcohols and other compounds using several force field models.

The SPC-Fw model does a good job of reproducing the experimental value of the static dielectric constant without much need for correction. It works better at lower temperatures and worsens slightly as the temperature increases. Applying the correction with a scaling factor of $k = 1.005$ leads to a minor improvement of the results. For the TIP4P model, a charge scaling factor of $k = 1.229$ leads to a good agreement of the simulation data with experimental observations.

An interesting consequence of our charge scaling approach is that it allows us to estimate the dipole moment of the molecules in the liquid phase, by applying Eq. (2) in reverse. Using the values in Table 1, we obtain a dipole of 2.66 D for ethanol in the liquid phase. Although we were not able to find any data for ethanol, high-level *ab initio* calculations for liquid methanol estimate a dipole moment of 2.7 ± 0.1 D[30,70], which agrees quite well with our estimate. For water, we estimate a liquid dipole of 2.35 D with SPC-Fw and 2.68 D with TIP4P. Experimental[71] and theoretical (see Ref. 72 and references therein) estimates place the liquid water dipole between 2.6 and 3.0 D. The TIP4P estimate is just

within this range, at the lower end, while the SPC-Fw estimate is much lower. Somewhat paradoxically, this is because it performs so well at predicting the dielectric constant with the bare fixed charges. However, this good performance is somewhat misleading, as it is inconsistent with the high liquid dipole moment observed experimentally and quantum mechanically.

From these systems, we find that the simple addition of the electronic polarizability with charge scaling allows simulations with force fields that were originally designed to reproduce thermodynamic properties to also accurately describe the static dielectric constant. This only requires the use of one parameter k, which will depend on the particular compound and the force field model; however, once the value of k is obtained, the entire temperature dependence of ε_0 can be predicted. This gives credibility to the idea that the charge that couples to an external electric field is not the same as that which governs the intermolecular interactions. In the next section, we test this idea in the case of mixtures.

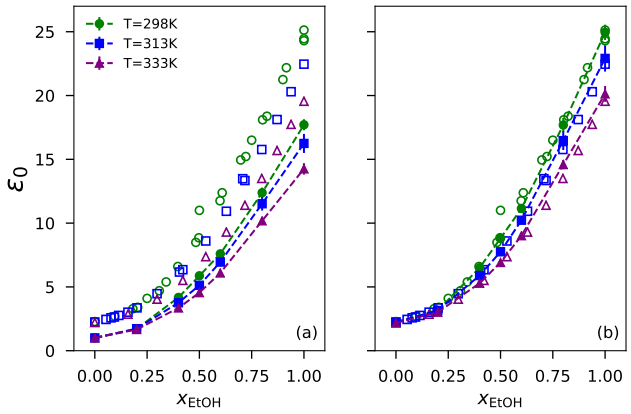

Fig. 2 The static dielectric constant ε_0 of ethanol-benzene mixtures at 298 K (green circles), 313 K (blue squares), and 333 K (violet triangles). The filled symbols are simulation data (a) before and (b) after applying the suggested correction scheme, and the open symbols are experimental data[49,57].

3.2 Mixtures

For the pure liquids examined in the previous section, we found that the simulation data could be rescaled to reproduce the experimental dielectric constant by adding the electronic polarizability and scaling the charges by a single, temperature independent constant k; however, this scaling constant is found to be dependent on the particular component and the particular force field model used. In this section, we examine the static dielectric constant of liquid mixtures, which pose an interesting challenge as to how to apply the correction.

We examine three different cases. The first is the ethanol-benzene mixture, where the scaling factor for the charge is only relevant for one of the components. In this case, it is unambiguous what value to choose for k, and we choose the pure ethanol value. The second system is the ethanol mixtures with TIP4P water. In this case, the scaling factor of both the pure components differ, although their values are fairly similar. The final system is the mixture of ethanol with SPC-Fw water. Here, the two components have a more substantial difference in k, where for the SPC-Fw model it is close to 1.

3.2.1 Ethanol-benzene mixtures.

The static dielectric constant of ethanol-benzene mixtures at different temperatures is shown in Fig. 2(a), where the open symbols are experimental data and the filled symbols are the MD simulation data. As with the pure component systems, the simulation results lie consistently beneath experimentally measured values. Due to the symmetry of the molecule, benzene has a negligible dipole moment. Consequently, scaling the charges of the benzene molecule will not affect the predicted dielectric constant. This suggests that we use the value of $k = 1.176$ for ethanol.

The electronic polarizability of the mixture is expected to be made up of the polarizabilities of the individual molecules in the system. As mentioned in the previous section, the influence of the electronic polarizability is directly related to the ability of the electron distribution of the individual molecules to deform in response to an externally applied electric field. As a first approximation, one would expect that the electronic polarizability of a mixture would be directly related to the polarizability of each molecular species, weighted by its volume fraction[73]. The electronic contribution to the dielectric constant ε_∞ to be used in Eq. (3) is then given by

$$\frac{\varepsilon_\infty - 1}{\varepsilon_\infty + 2} = \frac{4\pi}{3} \sum_\alpha \rho_\alpha^\circ \chi_\alpha \phi_\alpha, \tag{6}$$

where ρ_α° is the number density of a system of pure α, χ_α is the electronic polarizability of molecules of type α, ρ_α is their number density in the system, and $\phi_\alpha = \rho_\alpha v_\alpha$ is their volume fraction in the mixture.

To compute the volume fractions, the volume v_α occupied by each type of molecule must be assigned. In solutions with non-ideal mixing, there is ambiguity in how to divide the system volume between the various components. One manner to do this is to use the partial molar volumes $\bar{V}_\alpha$ (i.e. set $v_\alpha = \bar{V}_\alpha$), which are defined as:

$$\bar{V}_\alpha = \left(\frac{\partial V}{\partial N_\alpha} \right)_{T,p,N_{\alpha' \neq \alpha}}. \tag{7}$$

Equation (6) can be rearranged to give:

$$\varepsilon_\infty = 1 + \frac{4\pi \sum_\alpha \rho_\alpha^\circ \chi_\alpha \phi_\alpha}{1 - 4\pi \sum_\alpha \rho_\alpha^\circ \chi_\alpha \phi_\alpha / 3}. \tag{8}$$

This infinite frequency correction to the static dielectric constant can be quantified using the refractive index. In fact, the index of refraction has been explored as a manner to experimentally determine[74] the excess molar volumes of the different components in a solution, such as in alcohol-water mixtures[75], hydrocarbon-alcohol mixtures[76], and other solutions[77–79].

For the systems that we examine, the excess volume of mixing is relatively small. For solutions with little to no volume change on mixing, the partial molar volume of a molecule is approximately equal to its volume in the pure state (i.e. $v_\alpha = \bar{V}_\alpha \approx 1/\rho_\alpha^\circ$). In this

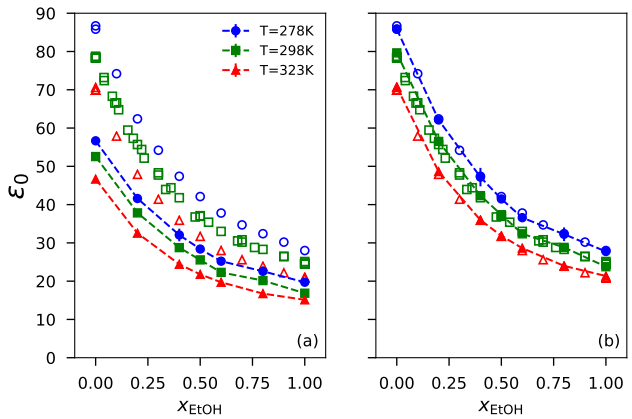

Fig. 3 The static dielectric constant ε_0 of ethanol (TraPPE-UA) / water (TIP4P) solutions at 278 K (blue circles), 298 K (green squares), and 323 K (red triangles). The filled symbols are simulation data (a) before and (b) after applying the suggested correction scheme, and the open symbols are experimental data [44–53].

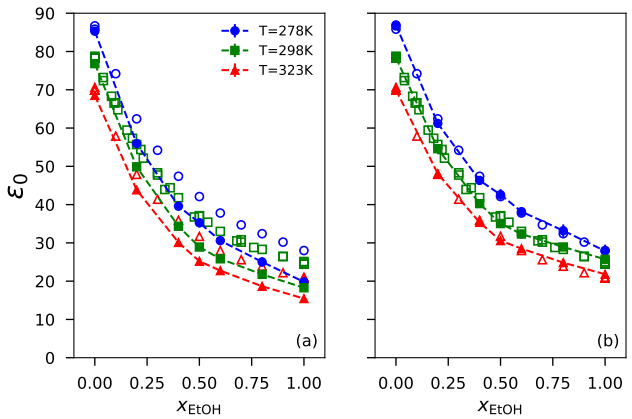

Fig. 4 The static dielectric constant ε_0 of ethanol (TraPPE-UA) / water (SPC-Fw) solutions at 278 K (blue circles), 298 K (green squares), and 323 K (red triangles). The filled symbols are simulation data (a) before and (b) after applying the suggested correction scheme, and the open symbols are experimental data [44–53].

case, Eq. (8) reduces to

$$\varepsilon_\infty = 1 + \frac{4\pi\rho\sum_\alpha x_\alpha \chi_\alpha}{1 - 4\pi\rho\sum_\alpha x_\alpha \chi_\alpha/3}, \tag{9}$$

where ρ is the number density of the mixture, and x_α is the mole fraction of component α in the mixture. The densities obtained from MD simulations for the mixtures studied in this work are reported in Fig. S5 of the ESI†. The resulting correction to the simulation predictions for the static dielectric constant is shown in Fig. 2(b). Excellent agreement with the experimental values is seen.

An even simpler approximation for ε_∞ can be obtained if we further linearize Eq. (8) with respect to the electronic polarizabilities, which then gives

$$\varepsilon_\infty = \sum_\alpha x_\alpha \varepsilon_{\alpha,\infty}, \tag{10}$$

where $\varepsilon_{\alpha,\infty}$ is the electronic dielectric constant of pure component α. We note that for the ethanol-benzene mixtures that we examined, the use of this approximation does not lead to noticeably different results from the more complicated expression given in Eq. (9). This is, in part, because the main contribution to the correction is the charge scaling effect.

3.2.2 Ethanol - TIP4P water.

The static dielectric constant for ethanol-water mixtures at various temperatures is shown in Fig. 3(a). The open symbols are experimental measurements, and the filled symbols are the results from MD simulations using the TraPPE-UA force field for ethanol and the TIP4P model for water. The simulation results consistently lie beneath the experimental values, as was the case for the pure systems.

The charge scaling factors differ for both pure component systems (i.e. $k = 1.176$ for ethanol and $k = 1.229$ for TIP4P water, see Table 1), although their values are not too dissimilar. When these two components are mixed, it is not entirely clear as to what value to choose for k. One assumption is that the charge scaling factors found in the pure component simulations still apply to each of the individual molecules. Then, the net system dipole moment for every saved configuration in the simulation trajectory is computed by scaling the charges on each molecule according to their value of k. The static dielectric constant is then recalculated over the original trajectory as the sum of the mean square net dipole moment of the system and the electronic polarization contribution (see Eq. (3)). While this is certainly feasible, here we examine the much less computationally intensive approximation where the dipole correlations between each pair of components is the same.

If we assume that the orientational dipole correlations between molecules of different species, as quantified by the Kirkwood g-factor [80], are similar, then the scaling factor for the mixture will take the form:

$$k = \sum_\alpha x_\alpha k_\alpha. \tag{11}$$

where k_α is the charge scaling factor for pure component α. Using this mixing rule and the previous mixing rule for ε_∞ (see Eq. (9)), the corrected simulation predictions for the static dielectric constant are shown in Fig. 3(b). As can be seen, this leads to excellent agreement between simulation results and the experimentally measured values across the entire composition range, validating the above approximation.

3.2.3 Ethanol - SPC-Fw water.

Finally, we examine the predictions for the static dielectric constant for ethanol-water mixtures, where the water is modelled using the SPC-Fw force field. This is a more stringent test to our mixing rule for k, since the scaling constants for the two components are significantly different. A comparison of the simulation results with experimental data is shown in Fig. 4(a). The results are as expected, based on the results for the one component systems. For pure water, which has $k = 1.005$, the simulation predictions are in close agreement with the experimental measurements. As the concentration of ethanol, which has $k = 1.176$, in the mixture increases, the simulation results underpredict the

dielectric constant.

In Fig. 4(b), the simulation data are corrected according to Eq. (3), with the mixture electronic polarizability given by Eq. (9) and the charge scaling factor given by Eq. (11). The agreement between the two is seen to be very good, confirming the conclusions obtained for the other two systems, and showing that the correction scheme also applies to systems with significantly different charge scaling factors.

4 Conclusions

Force fields based on effective pair potentials between molecules are commonly used to model materials. Most of these models have been developed specifically to reproduce thermodynamic properties and have been quite successful in describing a wide range of their static and dynamic properties. However, an important property that these models have found difficult to accurately and consistently predict is the static dielectric constant, which characterizes a system's response to an applied electric field. This is mainly a result of the manner in which the electric polarizability effects are included in the parameters of the force field and the limited ability of pairwise additive interactions to reproduce the true potential energy surface of realistic systems. The charge distribution of a molecule depends on its environment, due to the electrostatic potential generated by neighboring molecules and any applied electric fields. This environment fluctuates, with the continuous reconfiguration of neighboring molecules from their thermal motion, and, consequently, the charge distribution on a molecule also fluctuates. In pairwise additive force field models, the mobility of the electronic density of the molecules is only indirectly accounted for by assigning fixed values of effective charges at sites within the molecules; the charge density is rigid and reflects the average environment that it experiences.

As a result of this, there are two main effects that determine the dielectric constant which are neglected: the direct polarization of the electron distribution of molecules by an applied electric field, and the coupling of the charges on the molecules to the applied electric field which cause their rotation and translation. To account for these effects, it was previously proposed that the predictions for the dielectric constant by pairwise additive force fields could be significantly improved by accounting for the contribution from electronic polarization and scaling the charges in the force field. In this work, we further explore how this proposed correction performs under more general conditions, specifically the influence of temperature and composition.

The proposed corrections appear to properly capture the temperature dependence of the static dielectric constant. While the simulation data for the systems that we examined qualitatively followed the experimentally measured values, they typically underpredicted the value. With the correction, the simulation predictions were found to quantitatively agree with the experimental values across the entire ranges of temperature and composition. The electronic contribution to the dielectric constant ε_∞ can be estimated from the experimental electronic polarizability or the refractive index of the system at the sodium D-line. Only one fit parameter, the charge scaling factor k, is required for each pure component at a single temperature to implement the correction; this was found to be independent of temperature, at least for the conditions that we examined. The precise value of the scaling factor is dependent on the particular force field used to represent the molecule. Different force fields may require different values of k. An example is water, where the SPC-Fw model has $k \approx 1.005$ and TIP4P has $k \approx 1.229$.

An interesting question is how the charge scaling factor depends on the phase of the system. Vega and co-workers[81] have analyzed the static dielectric constant of various ice phases from various pairwise additive force field models for water. For the TIP4P/2005 model[82], they find that a scaling factor of $k \approx 1.15$ provides a good description of the liquid phase dielectric constant, while $k \approx 1.44$ provides a good agreement between the simulation results and experimental measurements for the ice Ih and ice III phases at 243 K over the range of pressures examined in the paper.

We also examined the performance of the correction for ethanol-benzene and ethanol-water mixtures. For these systems, we find that simple "mixing rules" could be applied to the pure component polarizabilities and charge scaling factors, thus extending our approach to liquid mixtures. There is no need to employ any additional fitting parameters. This approach led to very good agreement between the corrected simulation predictions and the experimental measurements, including systems where the pure components have very different values of charge scaling factor.

The systems that we examined in this work do not exhibit significant volume changes on mixing, and, consequently, we were unable to fully explore the ability of different mixing rules to correct the predictions of the dielectric constant from molecular simulations of pairwise additive force fields. It would be interesting to examine these types of systems to better understand the applicability of different mixing rules.

Conflicts of interest

There are no conflicts to declare.

References

1 W. L. Jorgensen, D. S. Maxwell and J. Tirado-Rives, *J. Am. Chem. Soc.*, 1996, **118**, 11225–11236.

2 M. J. Robertson, J. Tirado-Rives and W. L. Jorgensen, *J. Chem. Theory Comput.*, 2015, **11**, 3499–3509.

3 M. G. Martin and J. I. Siepmann, *J. Phys. Chem. B*, 1998, **102**, 2569–2577.

4 M. G. Martin and J. I. Siepmann, *J. Phys. Chem. B*, 1999, **103**, 4508–4517.

5 C. D. Wick, M. G. Martin and J. I. Siepmann, *J. Phys. Chem. B*, 2000, **104**, 8008–8016.

6 B. Chen, J. J. Potoff and J. I. Siepmann, *J. Phys. Chem. B*, 2001, **105**, 3093–3104.

7 J. M. Stubbs, J. J. Potoff and J. I. Siepmann, *J. Phys. Chem. B*, 2004, **108**, 17596–17605.

8 C. D. Wick, J. M. Stubbs, N. Rai and J. I. Siepmann, *J. Phys. Chem. B*, 2005, **109**, 18974–18982.

9 N. Lubna, G. Kamath, J. J. Potoff, N. Rai and J. I. Siepmann, *J. Phys. Chem. B*, 2005, **109**, 24100–24107.

10 B. Chen and J. I. Siepmann, *J. Phys. Chem. B*, 1999, **103**, 5370–5379.

11 N. Rai and J. I. Siepmann, *J. Phys. Chem. B*, 2007, **111**, 10790–10799.

12 J. Huang, S. Rauscher, G. Nawrocki, T. Ran, M. Feig, B. L. de Groot, H. Grubmüller and A. D. MacKerell, *Nat. Methods*, 2016, **14**, 71–73.

13 W. D. Cornell, P. Cieplak, C. I. Bayly, I. R. Gould, K. M. Merz, D. M. Ferguson, D. C. Spellmeyer, T. Fox, J. W. Caldwell and P. A. Kollman, *J. Am. Chem. Soc.*, 1995, **117**, 5179–5197.

14 W. D. Cornell, P. Cieplak, C. I. Bayly, I. R. Gould, K. M. Merz, D. M. Ferguson, D. C. Spellmeyer, T. Fox, J. W. Caldwell and P. A. Kollman, *J. Am. Chem. Soc.*, 1996, **118**, 2309–2309.

15 C. Oostenbrink, A. Villa, A. E. Mark and W. F. Van Gunsteren, *J. Comput. Chem.*, 2004, **25**, 1656–1676.

16 M. Martínez-Jiménez and H. Saint-Martin, *J. Chem. Theory Comput.*, 2018, **14**, 2526–2537.

17 F. J. Salas, G. A. Méndez-Maldonado, E. Núñez Rojas, G. E. Aguilar-Pineda, H. Domínguez and J. Alejandre, *J. Chem. Theory Comput.*, 2015, **11**, 683–693.

18 K. A. Beauchamp, J. M. Behr, A. S. Rustenburg, C. I. Bayly, K. Kroenlein and J. D. Chodera, *J. Phys. Chem. B*, 2015, **119**, 12912–12920.

19 C. J. Fennell, L. Li and K. A. Dill, *J. Phys. Chem. B*, 2012, **116**, 6936–6944.

20 C. Caleman, P. J. van Maaren, M. Hong, J. S. Hub, L. T. Costa and D. van der Spoel, *J. Chem. Theory Comput.*, 2011, **8**, 61–74.

21 M. Neumann and O. Steinhauser, *Chem. Phys. Lett.*, 1983, **102**, 508–513.

22 M. P. Allen and D. J. Tildesley, *Computer Simulation of Liquids*, Clarendon Press, New York, NY, USA, 1989.

23 C. Vega, *Mol. Phys.*, 2015, **113**, 1145–1163.

24 I. V. Leontyev and A. A. Stuchebrukhov, *J. Chem. Phys.*, 2009, **130**, 085102.

25 I. Leontyev and A. Stuchebrukhov, *Phys. Chem. Chem. Phys.*, 2011, **13**, 2613.

26 I. V. Leontyev and A. A. Stuchebrukhov, *J. Chem. Phys.*, 2014, **141**, 014103.

27 P. G. Karamertzanis, P. Raiteri and A. Galindo, *Journal of Chemical Theory and Computation*, 2010, **6**, 1590âĂŞ1607.

28 D. S. Cerutti, J. E. Rice, W. C. Swope and D. A. Case, *The Journal of Physical Chemistry B*, 2013, **117**, 2328âĂŞ2338.

29 D. J. Cole, J. Z. Vilseck, J. Tirado-Rives, M. C. Payne and W. L. Jorgensen, *Journal of Chemical Theory and Computation*, 2016, **12**, 2312âĂŞ2323.

30 M. C. Barrera and M. Jorge, *J. Chem. Inf. Model.*, 2020, **60**, 1352–1367.

31 M. Jorge and L. Lue, *J. Chem. Phys.*, 2019, **150**, 084108.

32 J. Cardona, R. Fartaria, M. B. Sweatman and L. Lue, *Mol. Simul.*, 2016, **42**, 370–390.

33 J. Cardona, M. B. Sweatman and L. Lue, *J. Phys. Chem. B*, 2018, **122**, 1505–1515.

34 P. Zarzycki and B. Gilbert, *Phys. Chem. Chem. Phys.*, 2020, **22**, 1011 1018.

35 W. L. Jorgensen, J. Chandrasekhar, J. D. Madura, R. W. Impey and M. L. Klein, *J. Chem. Phys.*, 1983, **79**, 926–935.

36 Y. Wu, H. L. Tepper and G. A. Voth, *J. Chem. Phys.*, 2006, **124**, 024503.

37 C. Vega and J. L. F. Abascal, *PCCP*, 2011, **13**, 19663.

38 E. Lindahl, M. Abraham, B. Hess and D. van der Spoel, *GROMACS 2019.3 Source code*, 2019, `https://zenodo.org/record/3243833`.

39 G. Bussi, D. Donadio and M. Parrinello, *J. Chem. Phys.*, 2007, **126**, 014101.

40 M. Parrinello and A. Rahman, *J. Appl. Phys.*, 1981, **52**, 7182–7190.

41 S. Nose and M. Klein, *Mol. Phys.*, 1983, **50**, 1055–1076.

42 U. Essmann, L. Perera, M. L. Berkowitz, T. Darden, H. Lee and L. G. Pedersen, *J. Chem. Phys.*, 1995, **103**, 8577–8593.

43 B. Hess, H. Bekker, H. J. C. Berendsen and J. G. E. M. Fraaije, *J Comput. Chem.*, 1997, **18**, 1463–1472.

44 D. E. Buck, *Ph.D. thesis*, Massachusetts Institute of Technology. Dept. of Chemistry., 1965.

45 H. Kienitz and K. N. Marsh, *Pure Appl. Chem.*, 1981, **53**, 1847–1862.

46 U. Kaatze, *J. Chem. Eng. Data*, 1989, **34**, 371–374.

47 W. Ellison, K. Lamkaouchi and J.-M. Moreau, *J. Mol. Liq.*, 1996, **68**, 171–279.

48 T. Sato and R. Buchner, *J. Phys. Chem. A*, 2004, **108**, 5007–5015.

49 R. Sengwa, Madhvi, S. Sankhla and S. Sharma, *J. Solution Chem.*, 2006, **35**, 1037–1055.

50 W. Dannhauser and L. W. Bahe, *J. Chem. Phys.*, 1964, **40**, 3058–3066.

51 M. Khimenko, V. Aleksandrov and N. Gritsenko, *Russ. J. Phys. Chem.*, 1973, **47**, 2914–2915.

52 P. Petong, R. Pottel and U. Kaatze, *J. Phys. Chem. A*, 2000, **104**, 7420–7428.

53 A. Gregory and R. N. Clarke, *Tables of the complex permittivity of dielectric reference liquids at frequencies up to 5 GHz.*, National Physical Laboratory NPL Report MAT 23, 2012.

54 J. F. King and W. A. Patrick, *J. Am. Chem. Soc.*, 1921, **43**, 1835–1843.

55 F. R. Goss, *J. Chem. Soc.*, 1940, **0**, 888–894.

56 B. M. Fridman, *Russ. J. Phys. Chem.*, 1975, **49**, 1423–1424.

57 G. Starobinets, K. Starobinets and L. Ryzhikova, *Zh. Fiz. Khim.*, 1951, **25**, 1186–1197.

58 M. Sprik, *J. Chem. Phys.*, 1991, **95**, 6762–6769.

59 M. Sharma, R. Resta and R. Car, *Phys. Rev. Lett.*, 2007, **98**, 247401.

60 J.-Z. Bao, M. L. Swicord and C. C. Davis, *J. Chem. Phys.*, 1996, **104**, 4441–4450.

61 P. Petong, R. Pottel and U. Kaatze, *J. Phys. Chem. A*, 1999, **103**, 6114–6121.

62 M. Dzida and U. Kaatze, *J. Phys. Chem. B*, 2015, **119**, 12480–12489.

63 T. N. Olney, N. M. Cann, G. Cooper and C. E. Brion, *Chem. Phys.*, 1997, **223**, 59–98.

64 Y. Marcus, *The Properties of Solvents*, Wiley, 1998, p. 254.

65 R. Bosque and J. Sales, *J. Chem. Inf. Comput. Sci.*, 2002, **42**, 1154–1163.

66 M. Gussoni, M. Rui and G. Zerbi, *J. Mol. Struct.*, 1998, **447**, 163–215.

67 J. Ralph D. Nelson, J. David R. Lide and A. A. Maryott, *Selected Values of Electric Dipole Moments for Molecules in the Gas Phase*, National bureau of standards technical report, 1967.

68 O. F. Mossotti, *Mem. di Mathem. e Fisica in Modena*, 1850, **24**, 49–743.

69 R. Clausius, *Die Mechanische Behandlung der Electricität*, 1879, 62–97.

70 N. Sieffert, M. Bühl, M.-P. Gaigeot and C. A. Morrison, *J. Chem. Theory Comput.*, 2012, **9**, 106–118.

71 Y. S. Badyal, M. Saboungi, D. L. Price, S. D. Shastri, D. R. Haeffner and A. K. Soper, *J. Chem. Phys.*, 2000, **112**, 9206–9208.

72 A. W. Milne and M. Jorge, *J. Chem. Theory Comput.*, 2019, **15**, 1065–1078.

73 C. J. F. Bottcher, *Theory of Electric Polarization*, Elsevier, Amsterdam, 2nd edn., 1973.

74 A. Z. Tasic, B. D. Djordjevic, D. K. Grozdanic and N. Radojkovic, *J. Chem. Eng. Data*, 1992, **37**, 310–313.

75 J. Herráez and R. Belda, *J. Solution Chem.*, 2006, **35**, 1315–1328.

76 R. Mehra, *J. Chem. Sci.*, 2003, **115**, 147–154.

77 A. Ali and M. Tariq, *Chem. Eng. Commun.*, 2007, **195**, 43–56.

78 M. Gupta, I. Vibhu and J. P. Shukla, *Phys. Chem. Liq.*, 2010, **48**, 415–427.

79 R. K. Shukla, A. Kumar, U. Srivastava, K. Srivastava and V. S. Gangwar, *Arabian J. Chem.*, 2016, **9**, S1357–S1367.

80 J. G. Kirkwood, *J. Chem. Phys.*, 1939, **7**, 911–919.

81 J. L. Aragones, L. G. MacDowell and C. Vega, *J. Phys. Chem. A*, 2011, **115**, 5745–5758.

82 J. L. F. Abascal and C. Vega, *J. Chem. Phys.*, 2005, **123**, 234505.